Development of a homodyne mixing system for performance characterization of terahertz superconducting KIDs

ZHANG Jia-Wen[1,2*], JIN Jun-Da[2], SHI Sheng-Cai[2], LI Jing[2], GENG Wei[1,2], LYU Wei-Tao[3], LI Zhi[2], ZHI Qiang[1,2], PENG Zhao-Hang[1,2]

（1. School of Astronomy and Space，University of Science and Technology of China，Hefei 230026，China；
2. Purple Mountain Observatory，Chinese Academy of Sciences，Nanjing 210009，China；
3. Department of Physics，Chinese University of Hong Kong，Hong Kong 999077，China）

Abstract：The homodyne mixing system is used to characterizing the performance of terahertz superconducting kinetic inductance detectors（KIDs）. However，homodyne mixing systems still have issues such as mixer imbalance，measurement system integration，and interference signals. The author designed a new single channel homodyne mixing hardware system and software algorithms to achieve integration of the measurement system，calibration of IQ-mixer imbalance，and performance characterization of KID；Furthermore，noise measurement of KIDs in VNA（vector network analyzer）CW mode is achieved；Finally，the method of hardware circuit design by dual channel homodyne mixing system based on autocorrelation algorithm effectively suppresses interference signals. It is worth noting that these research results are applied to characterize the performance of KIDs，which is important in the design of KIDs arrays.

Key words：KIDs，homodyne mixing system，terahertz，autocorrelation

太赫兹超导动态电感探测器性能表征用零差混频系统研制

张嘉文[1,2*]，金骏达[2]，史生才[2]，李 婧[2]，耿 伟[1,2]，吕伟涛[3]，李 陟[2]，
支 强[1,2]，彭昭航[1,2]

（1. 中国科学技术大学 天文与空间学院，安徽 合肥 230026；
2. 中国科学院 紫金山天文台，江苏 南京 210009；
3. 香港中文大学 物理系，中国 香港 999077）

摘要：零差混频系统（Homodyne mixing system）对太赫兹超导动态电感探测器（Kinetic inductance detectors，KIDs）性能表征具有重要的作用。然而，零差混频系统仍存在混频器不平衡性、测量系统集成、干扰信号等问题。作者设计新型的单通道零差混频硬件系统，结合软件算法实现了测量系统的集成化、IQ混频器不平衡性校准、KID 的性能表征；同时实现了在 VNA(vector network analyzer)CW 模式下的 KIDs 噪声测量；以及基于自相关算法的双通道零差混频硬件电路设计，有效地抑制了干扰信号。值得注意的是，这些研究成果被应用于表征 KIDs 性能，对 KIDs 阵列设计起到了重要的作用。

关 键 词：KIDs；零差混频系统；太赫兹；自相关算法

中图分类号：O43   **文献标识码**：A

Introduction

The terahertz band（0. 1-10 THz）have numerous characteristics，such as high resolution，penetrability[1]，coherence[2]，transience[3]，molecular absorption and dispersion[4]，which have found wide applications in astronomy. After the Big Bang，the peak of the cosmic microwave background（CMB）radiation[5] and almost half of the photon energy in the universe are in the terahertz frequency range[6]. Therefore，the terahertz frequency range holds significant importance in the study of the structure and origin of the universe[7].

KIDs is a type of superconducting terahertz detector with high sensitivity，which is sensitive in the ultraviolet to near-infrared range. Compared to semiconductor detectors，the advantages of KIDs in their operating wavelength range include no false counts（readout noise，dark current，and cosmic rays），intrinsic spectral resolution，high speed，and radiation resistance. Additionally，KIDs are more easily scalable into large detector arrays compared to other superconducting detectors for terahertz wavelengths.

After the fabrication of KIDs chips，corresponding testing systems are required to measure various parameters to characterize the performance of the detectors. Based on the working principle of KIDs，parameters such as S_{21}，power spectral density（PSD）of noise，and responsivity need to be measured. By processing the test parameters data using software algorithms，the noise equivalent power（NEP）of KIDs can be obtained. NEP is a critical indicator of the detector′s sensitivity，and high sensitivity is one of the most important performance metrics for detectors，because of detectors with high sensitivity can detect even weaker signals. For detecting distant celestial objects，the emitted signal power from these targets is extremely weak. Only high-sensitivity detectors like KIDs can detect such faint signals，meeting the requirements of astronomical observations. Therefore，it is crucial to measure the various performance parameters of KIDs before integrating them into astronomical detection systems[8-9].

The homodyne mixing technique is employed in the circuit system to characterize various aspects of KIDs′ performance，and the performance of the homodyne mixing system significantly influences the characterization of the detector′s performance. Designing a high-performance homodyne mixing system will enhance the accuracy of characterizing the detector′s performance，thus contributing to improving the overall design of the detection system. Moreover，the easiness of operation and integration improvement of the homodyne mixing system will facilitate rapid testing and design work for researchers and designers，thereby enhancing the efficiency of KIDs′ development. Due to the high sensitivity of KIDs itself，it is susceptible to external signal interference，and the homodyne mixing system inevitably introduces some interference. Designing a high-performance，convenient，highly integrated，and anti-interference homodyne mixing system is significant for the performance characterization，design，and testing of KIDs[10-12].

1　Principles of KIDs and Homodyne Mixing System

1. 1　KIDs

KIDs The detection principle of KIDs is shown in Fig. 1 . The incident photons，representing the detection signal，come into contact with the thin film on the surface of the KIDs. When the photon energy exceeds twice the superconductor energy gap，the Cooper pairs in the superconducting material break into two quasiparticles，releasing phonons. The increase in the number of quasiparticles alters the dynamic inductance and surface impedance of the superconducting resonator，causing the resonant frequency of the resonator to shift to the left，while the quality factor（Q-value）of the resonator decreases.
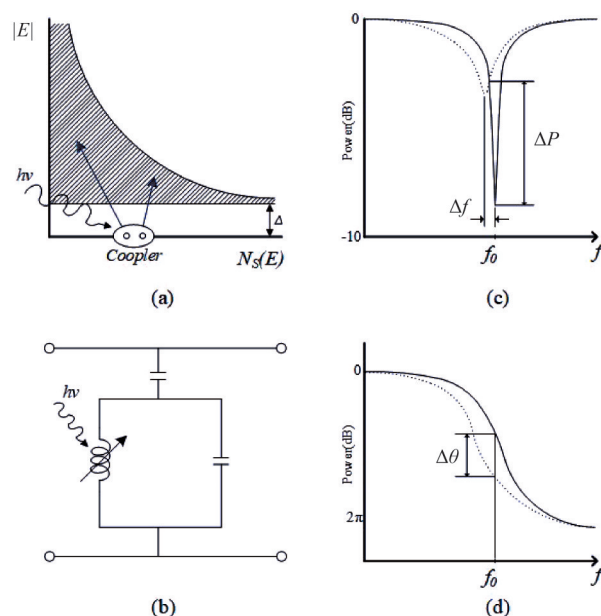

Fig. 1　Principle of KIDs′ detection
图 1　KIDs 的探测原理图

By characterizing the changes in the transmission properties of the superconducting transmission line coupled to the superconducting resonator，the variations in resonant frequency and phase can be obtained. Consequently，the energy of the incident photons can be derived，and signal detection can be accomplished through the conversion of physical property relationships. A typical physical representation of KIDs is shown in Fig. 2.

1. 2　Homodyne mixing system

The typical schematic diagram of the system using the homodyne mixing technique to characterize the performance of superconducting KIDs is shown in Fig. 3. This system primarily consists of a signal generator，directional coupler，IQ-mixer，low-pass filter，KIDs，low-temperature amplifier（HEMT），low-noise amplifier（LNA）operating at room temperature，ADC sampler，and other components.

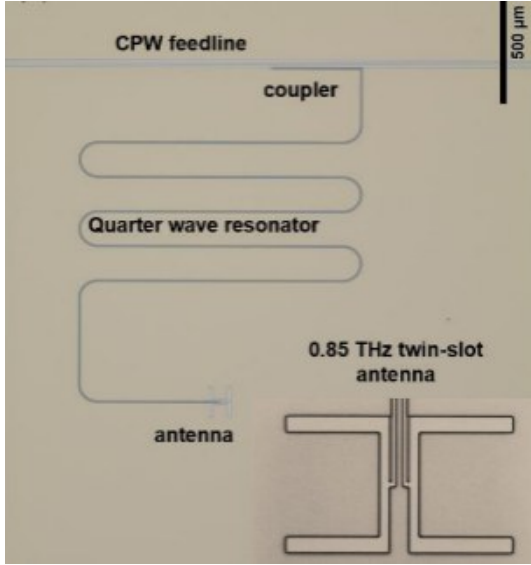The LO signal and the RF input are used as the in-

Fig. 2   Physical image of typical KIDs
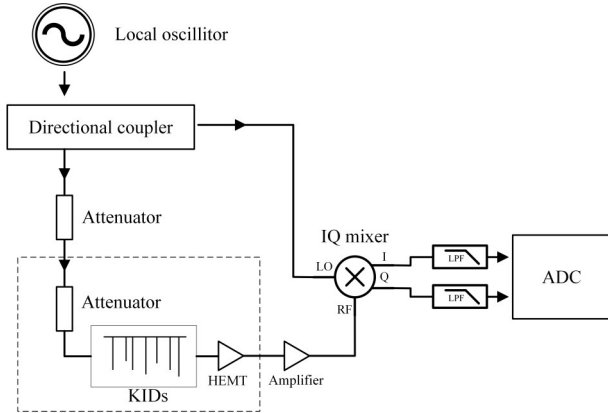图 2   典型 KIDs 的实物图

Fig. 3   Principle of homodyne mixing system structure for typical characterization of superconducting KIDs performance
图 3   典型表征超导 KIDs 性能用零差混频系统结构示意图

put signals for the IQ-mixer. The two ADC signals ($I(t)$ and $Q(t)$) obtained from the time-domain signals fed into sampling ports of the ADC through low-pass filters and impedance transformers. The two sampled time-domain signals are theoretically orthogonal signals and correspond to the set frequency f of the signal generator. After applying fast Fourier transform (FFT) to $I(t)$ and $Q(t)$, two sets of frequency-domain signals, I_{FFT} and Q_{FFT}, are obtained.

$$S_{21}(f) = I(t) + Q(t)*i \qquad , \quad (1)$$

$$\text{Amp}(f) = \text{FFT}\left(\sqrt{I(t)^2 + Q(t)^2}\right) \qquad , \quad (2)$$

$$\text{Phase}(f) = \text{FFT}\left(\arctan\left(\frac{I(t)}{Q(t)}\right)\right) \qquad , \quad (3)$$

The complex expression of S_{21} parameter for KIDs under working bandwidth can be expressed as formula (1). The amplitude (Amp) and phase (Phase) frequency domain signals of KIDs can be expressed as equations (2) and (3). The noise level of KIDs is characterized by

PSD. According to Parseval theorem and Wiener Khinchin theorem, the expression of PSD is formula (4), where $r(k)$ represents a discrete time series and N represents the length of the sequence (sampling rate * sampling duration). We can calculate the amplitude and phase PSD in the frequency domain through formula (4).

$$S_{xx}(f) = \frac{\text{FFT}(r(k))^2}{N} \qquad , \quad (4)$$

$$\text{NEP}(f) = \sqrt{S_{xx}(f)}\left(\frac{\text{d}A}{\text{d}P}\right)^{-1} \times \sqrt{1 + 2\pi f \tau_{\text{qp}}} \times$$
$$\sqrt{1 + 2\pi f \tau_{\text{res}}} \qquad , \quad (5)$$

After we get the PSD of KIDs, we only need to get the Responsivity of the resonance depth (A) of KIDs versus the input signal power (P), τ_{qp} and τ_{res} (response time of Quasiparticle and resonator), we can get the NEP representing the sensitivity of KIDs. The specific calculation is shown in Formula (5).

2   Hardware Design of Homodyne Mixing System

2.1   Homodyne mixing system

The schematic diagram of the designed homodyne circuit is shown in Fig. 4, which consists of a homodyne testing circuit module, a low-temperature KIDs testing equipment cryostat (located in the Dewar system), a digital sampling system (ADC) for signal collection and processing, and a vector network analyzer (VNA). During the test, the KIDs samples are placed in the refrigeration system cryostat, while other equipment operates at room temperature.

The signal input segment of the system comprises a 15 dB directional coupler and a microwave switch A, alongside a 90 dB adjustable attenuation attenuator, tailored to accommodate the local oscillator port's 15 dBm operating power. This setup ensures compatibility with the KIDs detectors, which typically handle signals below -80 dBm. In the homodyne mixing architecture, symmetry in signal frequency is essential for IQ-mixer operation, with one signal entering the local oscillator port and the other, after power adjustment, entering the Dewar. However, IQ-mixer imperfections like amplitude and phase imbalances necessitate calibration, termed IQ-Calibration. This process demands signals at similar frequencies to enter the mixer's LO and RF ports, facilitated by a microwave switch toggling between KIDs measurement and calibration.

In signal processing circuit, it revolves around two LNA stages, a 0-60 dB adjustable attenuator, and a microwave switch, with the IQ-mixer as its linchpin. A 90 dB adjustable attenuator precedes the RF signal's entry into the Dewar refrigeration system, housing the KIDs samples. The signal through internal attenuators, KIDs, and the low-temperature amplifier HEMT before undergoing amplification through the LNAs and attenuators. A 60 dB adjustable attenuator interposed between LNA stages serves two critical functions: preventing signal saturation in subsequent LNAs and ensuring linear operation of the IQ mixer by controlling input power. The sig-
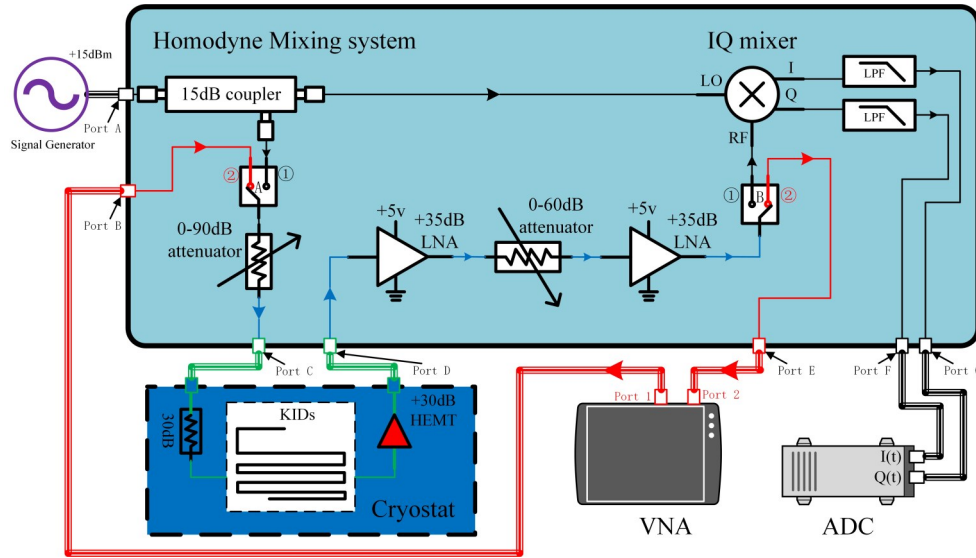
ZHANG Jia-Wen *et al*：Development of a homodyne mixing system for performance characterization of tera-
hertz superconducting KIDs

3 期

339

Fig. 4　Schematic diagram of single channel homodyne mixing system circuit
图 4　单通道零差混频系统电路原理图

nal generator feeds the LO port，while KIDs′ signal pass-es through LNA and attenuators before mixing，ideally generating two signals with matched amplitudes and a 90-degree phase difference.

Finally，the signal output and acquisition circuitry entail low-pass filters and impedance matching，dividing the IQ mixer′s output into I and Q channels. These sig-nals，along with ADC port connections，are managed through SMA lines and impedance matching. The ADC captures $I(t)$ and $Q(t)$ signals in the time domain for fur-ther processing.

Microwave switches A and B are devices of the same model，which can be controlled by an electronic control switch to switch between three working modes. <1>. ′Ho-modyne mixing mode′，when A switch is connected to 1 and B switch is connected to 1，homodyne forms a com-plete loop to measure the characteristics of KIDs；<2>. In the ′IQ-mixer calibration mode′，when the A switch is connected to 2 and the B switch is connected to 1，both the input and output Dewar ports are directly connected using SMA wires to form a calibration circuit. <3>. In the ′VNA mode′，when the A switch is connected to 2 and the B switch is connected to 2，the signal no longer passes through the mixer，but only the two-stage amplifi-er LNA and attenuator can be connected to VNA to mea-sure the S_{21} parameters of KIDs.

2.2　KIDs noise measurement based on VNA

when measuring the noise of KIDs to obtain their PSD，it is usually achieved using the homodyne mixer system. After studying the existing new VNA，we found that it can also achieve noise measurement for KIDs. We use Keysight′s model P5003A VNA，which can achieve vector network division mode，signal source mode，spec-trometer mode，and CW mode（time domain sampling）.

$$\Delta t = T - T_{\mathrm{Dwelltime}} * N_{\mathrm{SET}} \qquad , \quad (6)$$

$$f = N_{\mathrm{SET}} / \Delta t \qquad , \quad (7)$$

The hardware connection settings are as shown in

section 2.1 of the ′VNA mode′. VNA software is set to CW mode，setting the frequency to be tested，sampling duration，and observation points. The specific settings are shown in Fig. 5. Then open two test channels（chan-nal 1 and channal 2），set their test S_{21} parameters in units of ′imag′ and ′real′，and obtain the corresponding temporal sampling images，as shown in Fig. 6. Finally，we wrote special language SCPI command of test instru-ments and equipment to save hundreds of groups of data and facilitate the mean operation of subsequent software algorithm processing.
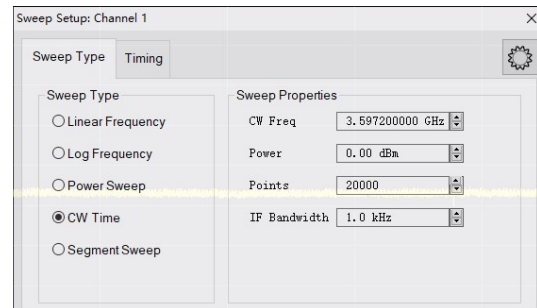

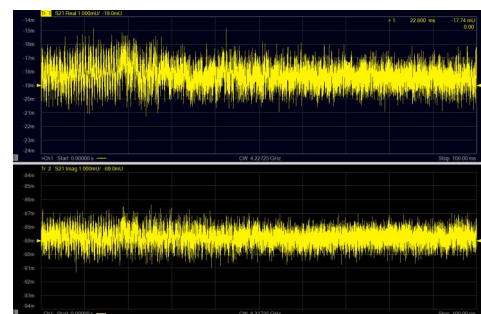Fig. 5　Setup window for VNA noise measurement in CW mode
图 5　VNA噪声测量CW模式下设置窗口

Fig. 6　Time domain interface between I and Q channels of VNA
图 6　VNA的I路与Q路时域界面

It should be noted that the observation points set by the VNA UI program are not the actual sampling points. The actual sampling points are related to the settings of VNA's' IF Bandwidth ',' Dwelltime ', sampling duration, and observation points (set by the instrument development company program). The sampling rate and sampling points of VNA cannot be set by the user, but can be calculated using formulas (6) and (7). (Δt is the actual sampling time interval, T is the set total sampling time, NSET is the total number of sampling points, and Dwelltime is the VNA dwell time). We changed the above parameters and calculated the sampling frequencies corresponding to different VNA settings, as shown in Table 1.

Table 1 Sampling frequency for different VNA settings
表 1 VNA不同设定的采样频率

N_{SET}	$T(ms)$	$T_{Dwell-time}(us)$	Actual sampling frequency(kHz)
20 000	100	1	250
20 000	300	11	250
20 000	1 000	46	250
40 000	200	1	250

Design of dual channel homodyne based on cross correlation operation

When we use a single channel homodyne mixing system based on Chapter 2. 1 to characterize their characteristics, there are the following problems：1. The noise collected by existing measurement systems is not only the noise of KIDs, but also the superposition of noise from amplifiers, attenuators, directional couplers, mixers, and other components of the KIDs readout system. KIDs is ultra-high sensitivity detectors, so noise generated by KIDs is lower than noise generated by some devices in the readout system will have a certain impact on measurement accuracy. 2. The measurement system will introduce external interference signals(such as 50 Hz frequency doubling signals, ADC interference signals, etc.) generated by other than KIDs. The common noise measurement systems cannot effectively solve this problem.

To solve the above problems, we used two single channel homodyne mixing systems combined with hardware testing methods of power splitters, as well as software cross correlation algorithms, to effectively suppress the noise generated by the homodyne mixing system and to some extent suppress interference signals. The specific hardware circuit is shown in Fig. 7.

The signal generator outputs a signal, which is divided into two channels by the directional coupler and these two signals enter into LO port of homodyne mixing system (LO1 and LO2). HMET amplifies the output signal of KIDs in the Dewar, and divides the output signal of HEMT into two identical signals as RF1 and RF2 through a power divider outside the Dewar. RF1 and LO1, as well as RF2 and LO2, are used as input signals for No. 1 and No. 2 homodyne mixing system, respectively. After output signals of two homodyne mixing system
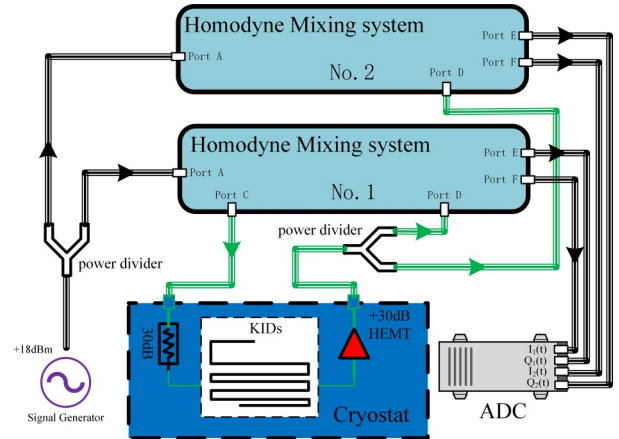

Fig. 7 Schematic diagram of dual channel homodyne mixing system circuit
图 7 双通道零差混频系统电路原理图

is mixed by IQ-mixer, the two time-domain signals are inputted into the ADC through an impedance converter. The signals are sampled as four ADC acquisition channels of dual channels $I_1(t)$ and $Q_1(t)$, $I_2(t)$ and $Q_2(t)$. Finally, the two-time domain signals are converted into amplitude or phase noise in the frequency domain through Autocorrelation and Fourier transform.

3 Software Algorithm Processing

3. 1 IQ mixer calibration

The two signals generated by an ideal IQ-mixer with the same amplitude and a phase difference of 90 ° can be represented by functions such as formulas (8) and (9)：

$$I = A \sin(\omega t) \qquad , \quad (8)$$
$$Q = A \cos(\omega t) \qquad , \quad (9)$$

Actually, the differences in device properties of IQ-mixer with RF frequency cause 3 problems：1. The amplitude imbalance；2. The phases imbalance 3. DC offset (between I and Q channels). This will cause errors in the noise measurement of KIDs. To eliminate this error, it is necessary to first correct the imbalance of the IQ-mixer, obtain the correction parameters for the imbalance, and then use these parameters to calibrate the KIDs measurement data at the corresponding frequency points to obtain accurate IQ two-way microwave signals.

According to section 2. 1, set the homodyne mixing system to the ' IQ-mixer calibration mode '. Two signal generators (one signal provided by the VNA of signal source mode) generate microwave signals close to the same frequency, one of which serves as an RF signal and the other as a local oscillator signal. The frequency settings of the two signal generators differ by a few kHz. Then use outputs data to draw an output circle (actually an ellipse before calibration), which is represented by the following two equations：

$$I = I_0 + A_I \sin \gamma \qquad , \quad (10)$$
$$Q = Q_0 + A_Q \cos \gamma \qquad , \quad (11)$$

Among them, I_0 and Q_0 (the center of the ellipse) represent the offset of the I and Q channel outputs, respectively；A_I/A_Q (the ratio of the major axis of an ellipse

to its minor axis) which is represented amplitude difference; γ which is the inclination angle of the ellipse, represents a fixed initial phase difference. The least squares ellipse fitting is introduced here to calibrate the imbalance of the IQ-mixer. The fitting method is given by the following equation (12)-(13), where N represents the number of sampling points.

$$F(A,B,C,D,E) = \sum_{i=1}^{N}(x_i^2 + Ax_iy_i + By_i^2 + Cx_i + DY_i + E)^2 \quad , \quad (12)$$

$$\frac{\partial F}{\partial A} = \frac{\partial F}{\partial B} = \frac{\partial F}{\partial C} = \frac{\partial F}{\partial D} = \frac{\partial F}{\partial E} = 0 \quad , \quad (13)$$

The five main parameters of the fitted ellipse, I_0, Q_0, A_I, A_Q, γ It can be represented by fitting parameters as formula (14)-(21), I_0 and Q_0 represent the DC offset of IQ-Mixer, A_I and A_Q represent the amplitude imbalance γ Characterizing phase offset.

$$I_0 = (BE - 2CD)/(4AC - B^2) \quad , \quad (14)$$

$$Q_0 = (BD - 2AE)/(4AC - B^2) \quad , \quad (15)$$

$$q = 0.5\arctan(B/(A - C)) \quad , \quad (16)$$

$$A_I = \sqrt{a^2\cos^2(q) + b^2\sin(q)} \quad , \quad (17)$$

$$A_Q = \sqrt{a^2\sin^2(q) + b^2\cos(q)} \quad , \quad (18)$$

$$\alpha_1 = \arctan[b\sin(q)/a\cos(q)] \quad , \quad (19)$$

$$\alpha_2 = \pi - \arctan[b\sin(q)/a\cos(q)] \quad , \quad (20)$$

$$\gamma = \alpha_1 - \alpha_2 \quad , \quad (21)$$

To obtain an ellipse fitted due to imbalance, we first need to correct the five parameters obtained in the previous section of the ellipse to a standard circle. Firstly, we deduct the DC offset (I-I_0, Q-Q_0) and return the corresponding ellipse center to the coordinate origin. Then calibrate the phase imbalance using the coordinate transformation formula shown in Fig. 8 It can be understood that an ellipse is obtained by performing coordinate amplitude and rotation transformations on a circle. We only need to invert the elliptical coordinates. Finally, we calibrate the amplitude imbalance, and the power of the dual ports before and after calibration should be conserved. The calibration of amplitude imbalance is based on the power conservation of the ports, as shown in formula (22), and the radius of the calibrated circle is R_{ref} (see formula (23)). The final calibration formula is shown in formulas (24) and (25).

$$\sqrt{a^2 + b^2} = \sqrt{R^2 + R^2} \quad , \quad (22)$$

$$R_{ref} = \sqrt{\frac{a^2 + b^2}{2}} \quad , \quad (23)$$

$$I_{CAL} = [(I - I_0) \times \cos\gamma + (Q - Q_0) \times \sin\gamma] \times R_{ref}/A_I , (24)$$

$$Q_{CAL} = [(Q - Q_0) \times \cos\gamma - (I - I_0) \times \sin\gamma] \times R_{ref}/A_Q \quad , \quad (25)$$

Fig. 9 shows the calibration images of the fitted ellipse before and after IQ calibration. From the figure, it can be seen that the calibrated I-channel and Q-channel meet the ideal IQ mixer characteristics under ideal conditions.

3.2 Seven parameter fitting

Due to the impedance mismatch of the test link, standing wave, signal transmission delay of the cable, and the quality factor of KIDs themselves, the resonant
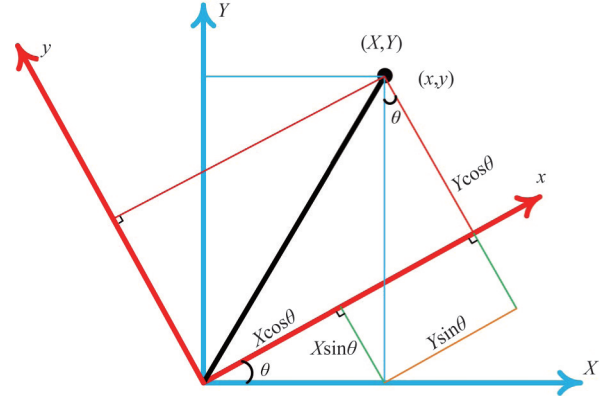

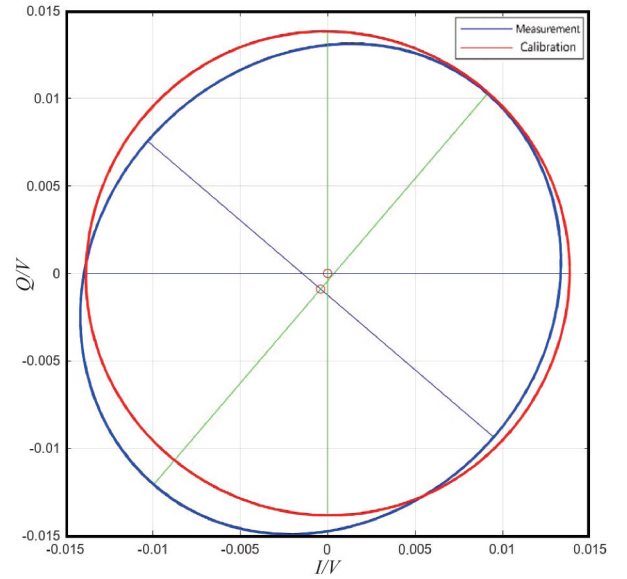Fig. 8 Diagram of coordinate rotation formula
图 8 坐标旋转公式图示

Fig. 9 Schematic diagram of IQ mixer calibration complex frequency domain
图 9 IQ混频器校准复频域示意图

characteristics of KIDs collected by ADC are different from the ideal resonant characteristics. According to the fitting data, the influence of these parameters on the resonant curve of KIDs can be eliminated. The equation of the S_{21} curve of the general KIDs resonator is Formula (26). The signals collected by ADC must first be fitted with 7 parameters.

$$S_{21}(f) = ae^{i\alpha}e^{-2\pi if\tau}\left[1 - \frac{(Q_l/|Q_c|e^{i\varphi})}{1 + 2iQ_l(f/f_r - 1)}\right], \quad (26)$$

$$S_{21}(f)_{cal} = \left(\frac{S_{21}(f)}{ae^{i\alpha}e^{-2\pi if\tau}} - 1\right)/e^{i\varphi} \quad , \quad (27)$$

Where f is the detection frequency, fr is the resonant frequency, Q_l is the load quality factor, and Q_c is the absolute value of the coupling quality factor, φ Indicates impedance mismatch, a is additional amplitude, α is phase shift, And electronic delay caused by cable length and limited speed of light τ。 The data collected by ADC was

fitted with seven parameters using the above formula, and then calibrated using formula （27） to obtain data that meets the general ideal resonance characteristics.

3. 3 Cross correlation algorithm

According to the content in Section 2. 3, the two-channel homodyne mixing system is used to sample the time domain data of the two channel I and Q channels through ADC, and four channel data of $I_1(t)$, $Q_1(t)$, $I_2(t)$ and $Q_2(t)$ as shown in Fig 10 are obtained through seven parameters fitting and calibration. The phase and amplitude time domain values are obtained, and Fast Fourier transform is performed. Then, for $A(f)$ and $\theta(f)$ Perform cross correlation operation （Xcor）, take the average of n sets of amplitude and phase noise data tested, and obtain the PSD of the first channel 1 FFT and the second channel 2 FFT corresponding to N groups of correlations through formula （28） operation.

The cross-correlation operation Xcor can effectively represent the noise generated by the same KIDs measured by a dual channel homodyne mixing system, while the noise generated by the measurement system is suppressed by the cross-correlation operation, thereby enhancing the accuracy of KIDs noise （PSD） characterization in the measurement system.

$$S_{XY} = \frac{1}{N} \left| \sum_{i=0}^{N-1} Y_i \cdot \mathrm{conj}(X_i) \right| \qquad , \quad (28)$$

4 Data Processing and Analysis

The Homodyne mixing system and KIDs settings are shown in the Fig. 11. HEMT and KIDs are installed on cold plates of 4 k and 50 mk levels respectively through blocks. Under normal temperature environment, ADC, VNA, and signal generator operate in different modes through the switch of the homodyne mixing system.

4. 1 Impact of IQ‑calibration on IQ‑Mixer linear interval

The linear operating range of the IQ mixer is an im-portant parameter for the entire homodyne system. When the KIDs output signals enter the linear range of the IQ Mixer, it is necessary to ensure that the signal does not experience distortion. We measured the input-output power curve of the IQ mixer by combining the signal source and spectrometer. We selected four frequency points of 2 GHz, 4 GHz, 6 GHz, and 8 GHz to test the corresponding RF input power/IQ output amplitude curves, where the output amplitude=20 log $\sqrt{(I_2+Q_2)}$. The measurement results are shown in Figs. 12-15.

After correction, the linear point of the IQ Mixer corresponding to the 2 GHz, 4 GHz, 6 GHz, and 8 GHz frequency points are 47 dB, 46 dB, 68 dB, and 56 dB, respectively. The uncalibrated curve has a narrow linear interval and singular inflection points. After calibration, the linear intervals are all greater than 45 dB, with a significant increase in linear intervals and no singular inflection points. The saturation power of the system on the right side of the linear region is approximately 5 dBm, and the output signal does not change as the input power increases. The bottom noise of the system is reached on the left side of the linear region, and does not change as the input signal strength decreases.

When the input power of the signal is too low, the output signal power will approach the DC offset. If the DC offset is negative and the curve monotonically increases or the DC offset is positive and the curve monotonically decreases, then the curve value will be squared and a turning point will appear. This explains the reason for the singular turning point in the linear interval of IQ Mixer corresponding to 2 GHz and 8 GHz frequency points. After IQ calibration, the DC offset is deducted and the inflection point does not exist.

4. 2 Measurement of S_{21} parameters and seven parameter fitting

The S_{21} of KIDs measured by the homodyne mixing system is shown in Fig 16. After seven parameter fitting,
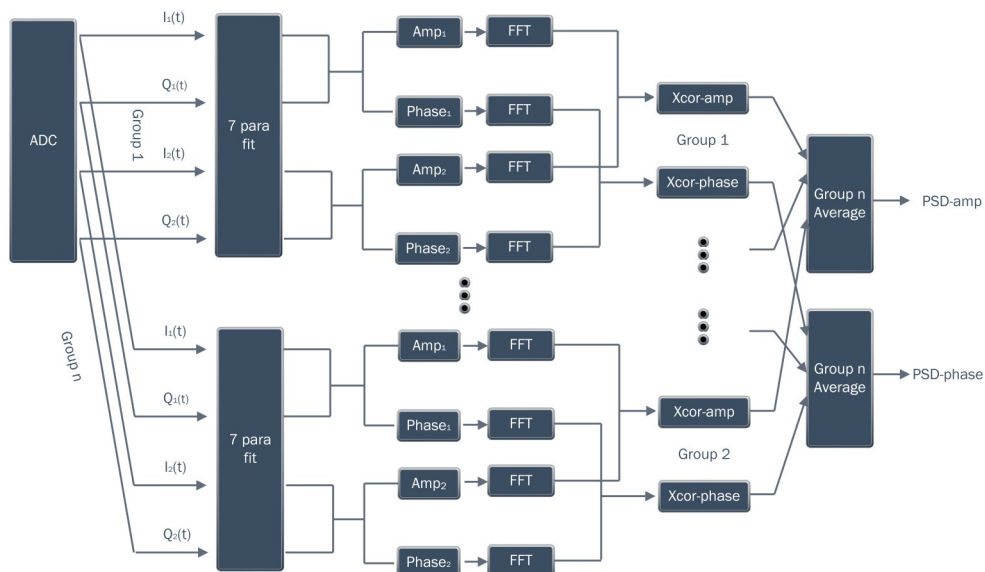

Fig. 10　Schematic diagram of cross correlation algorithm for dual channel homodyne mixing system
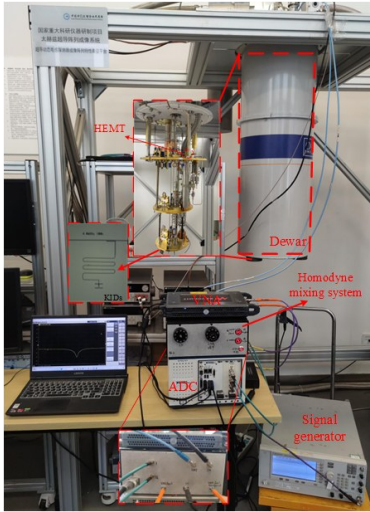
图 10　双通道homodyne mixing 系统互相关算法示意图

ZHANG Jia-Wen *et al*：Development of a homodyne mixing system for performance characterization of tera-
hertz superconducting KIDs

3 期   343

Fig. 11   The Homodyne mixing system and KIDs setup
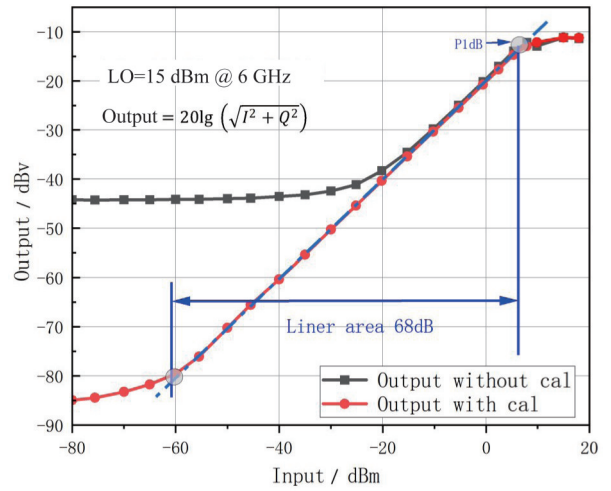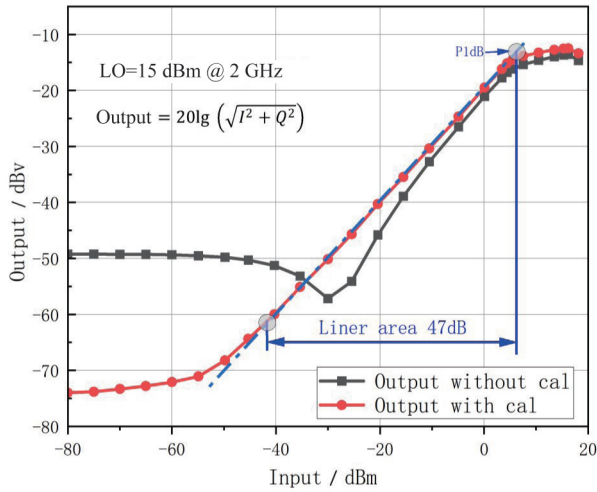图 11   Homodyne mixing 系统与KIDs设置如图

Fig. 12   IQ Mixer linear area @ 2 GHz
图 12   IQ-Mixer线性区间@2 GHz
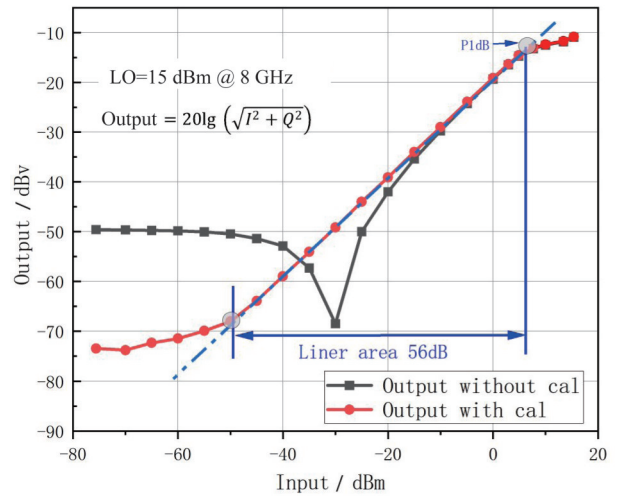

Fig. 13   IQ linear area @ 4 GHz
图 13   IQ-Mixer线性区间@4 GHz

Fig. 14   IQ Mixer linear area @ 6 GHz
图 14   IQ-Mixer线性区间@6 GHz

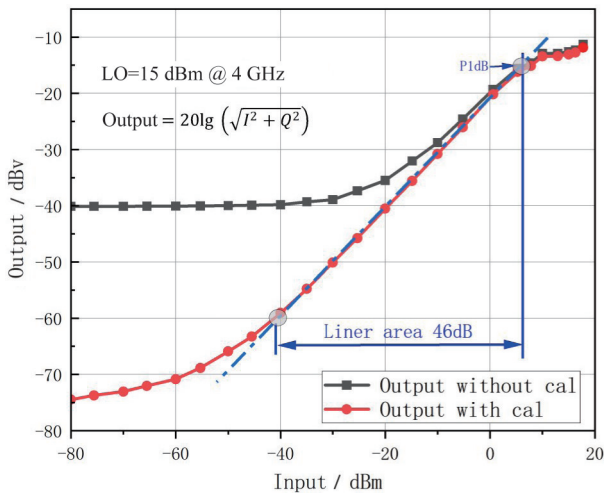Fig. 15   IQ Mixer linear area @ 8 GHz
图 15   IQ-Mixer线性区间@8 GHz

it can be seen that the resonance frequency is 4 035. 3 MHz,
the resonance depth is 22 dB，and the resonance circle
size is 0. 43 units. The resonance characteristic curve S_{21}
of KIDs is well characterized.

4. 3   PSD

We conducted time series sampling on the resonant
and non-resonant frequency points of KIDs resonators.
The non resonance were used to characterize the overall
noise level of the detection link，while the noise at the
resonance was used to characterize the noise level of the
detector. The collected noise is obtained from an ADC
with a sampling rate of 200 kHz and 20000 sampling
points.

We used the above method to perform temporal sam-
pling on the resonance and non-resonance of KIDs，fol-
lowed by IQ calibration and seven parameter fitting, and
finally obtained the PSD of the detector through Fourier
transform. Firstly，the time-domain signal of KIDs chips
with a resonant point of 4 186 MHz was measured using a
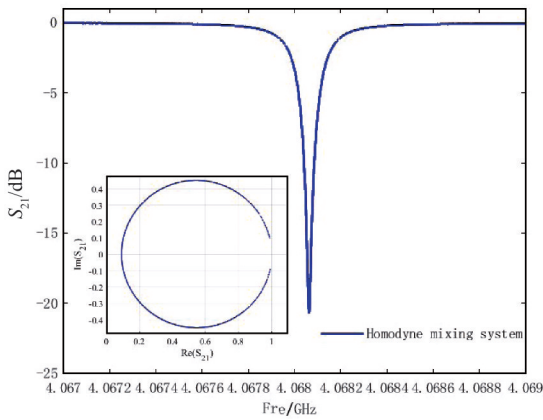single channel homodyne mixing system. Then，IQ-cali-

Fig. 16 S_{21} of KIDs measured by homodyne mixing system
图 16   homodyne mixing系统测得KIDs的S_{21}

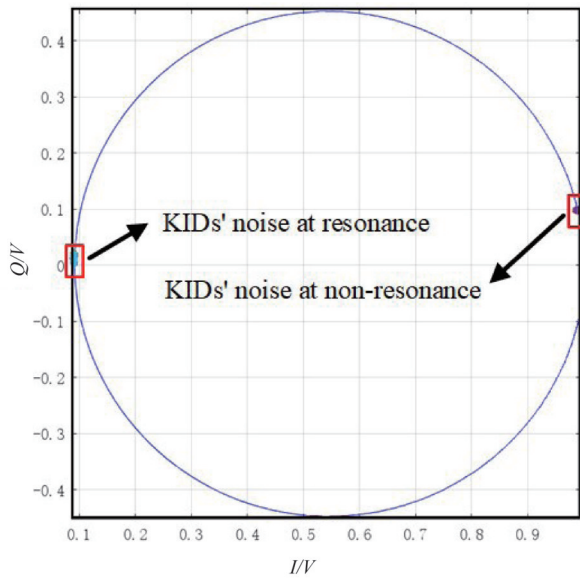
Fig. 17   Complex frequency domain diagram of KIDs resonance and non-resonance noise
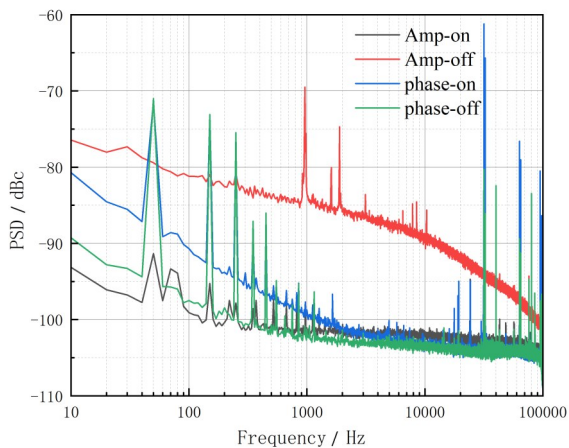图 17   KIDs谐振点与非谐振点噪声复频域图

Fig. 18   PSD of KIDs on resonance and non-resonance
图18   KIDs 谐振点与非谐振点PSD
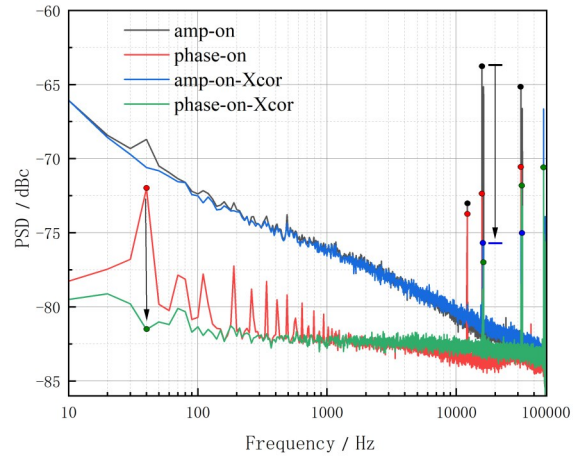

Fig. 19   Comparison of resonance PSD between single channel and dual channel homodyne system testing KIDs
图 19   单通道与双通道homodyne 系统测试KIDs谐振点PSD对比

bration and seven parameter fitting were performed on the noise points of the resonant and non-resonance. It can be seen that the resonance noise collected in the time domain of the resonance is plotted on the far-left side of the resonance circle graph, while the non-resonance is plotted in the area of the baseline (x-axis approaching 1) on the right side of the graph, as shown in Fig. 17. Then we further collected 500 sets of time-domain data from resonance and non-resonance to obtain the PSD of each set, and then averaged them to obtain the PSD of resonance and non-resonance, as shown in Fig. 18.

From the Fig. 18, it can be seen that the amplitude noise of the resonant point is higher than the phase noise, while the amplitude and phase noise of the non-resonant point are not significantly different, due to the characteristics of the resonant point itself. The overall noise of non-resonance is smaller than that of resonance, because the signal-to-noise ratio of non-resonance is better than that of resonance. However, the low-frequency 50 Hz interference signal and the signal generated by the high-frequency ADC. We obtained the PSD as shown in Fig. 19 through a dual channel cross correlation algorithm. It can be seen that the interference signal is well suppressed, and the baseline of the PSD curve of KIDs has not changed.

Based on the content of Chapter 2.2, we measured the noise of the aforementioned KIDs chips using VNA and obtained their PSD diagrams, as shown in Fig. 20. Compared to the PSD measured by the homodyne mixing system, the amplitude noise baseline of the KIDs chips measured by VNA is generally 3 dB larger, while the trend of phase noise variation is basically the same. This is because when VNA sets the sampling frequency, the setting of the intermediate frequency filter option (300 kHz) is larger than the low-pass filter (100 kHz) of the homodyne mixing system, which will introduce more noise.
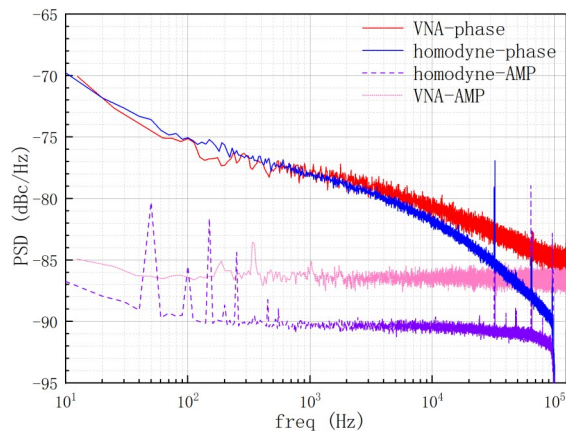
ZHANG Jia-Wen *et al*:Development of a homodyne mixing system for performance characterization of tera-
hertz superconducting KIDs

3 期

345

Fig. 20 KIDs PSD Test Result Graph Based on VNA
图 20 基于 VNA 的 KIDs PSD 测试结果图

4. 4 Responsivity and NEP

We obtained a curve of resonance depth with temperature by changing the temperature of the cryostat where KIDs are located, and fitted the values of dA/dT ($3.5 * 10^{-7}$) as shown in Fig. 21. Then, based on empirical formulas, we derived the curve dP/dT ($6×10^{-13}$) value of the detection signal power changing with temperature. Through the above formula with PSD measured by dual channel homodyne mixing system, we obtained the NEP value of KIDs, as shown in Fig. 22. Both of these values are very small and have a very small impact on NEP. From Figure 24, it can be seen that the minimum NEP of this KIDs is in the order of $1.2×10^{-18}$ (KIDs NEP theoretical limit 10^{-21}), and the sensitivity of this KIDs is well characterized.
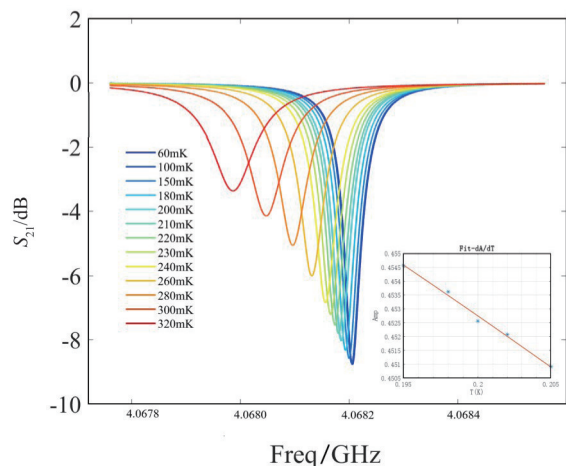

Fig. 21 S_{21} parameters of KIDs at different temperatures and DA/dT fitting curve
图 21 不同温度 KIDs 的 S_{21} 参数和 dA/dT 拟合曲线

5 Conclusion

This article designs a novel Homodyne mixing system to characterize the performance of KIDs. The newly designed single channel homodyne mixing hardware system facilitates IQ mixer calibration and integration with VNA through the combination of microwave switches and
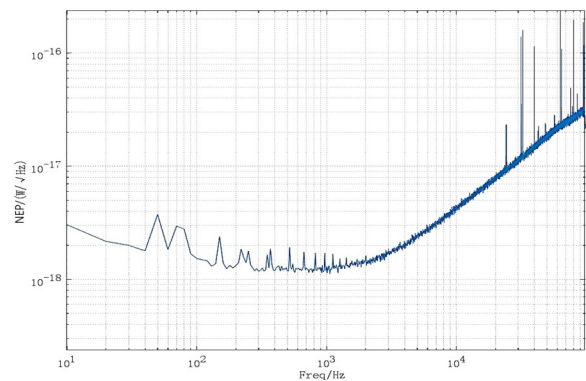

Fig 22 NEP result of KIDs
图 22 KIDs 的 NEP 结果图

other microwave devices；By combining the CW mode of the new VNA，the measurement of KIDs noise by VNA has been achieved；By designing a dual channel homodyne mixing system and combining it with dual channel algorithms，the influence of interference signals has been effectively suppressed. The software algorithm has achieved the calibration of IQ-mixer imbalance，expanding the linear range of the mixer to no less than 45 dB. These research results have been applied to characterize the performance of KIDs and have played an important role in the design of KIDs arrays.

References

[1] Cutting-edge terahertz technology | Nature Photonics [EB/OL]. / 2023-07-12. https://www.nature.com/articles/nphoton.2007.3.
[2] Dekorsy T, Auer H, Waschke C, et al. Emission of Submillimeter Electromagnetic Waves by Coherent Phonons. Phys Rev Lett. 1995 Jan 30;74(5):738-741
[3] (PDF) Integrated THz technology for label-free genetic diagnostics [EB/OL]. /2023-07-12. https://www. researchgate. net/publication/ 228075953_Integrated_THz_technology_for_label-free_genetic_di - agnostics.
[4] Woodward R M, Wallace V P, Pye R J. Terahertz pulse imaging of ex vivo basal cell carcinoma[J]. *The Journal of Investigative Dermatology*, 2003, **120**(1): 72 – 78.
[5] Wootten A, Thompson A R. The Atacama Large Millimeter/submillimeter Array[J]. *Proceedings of the IEEE*, 2009, **97**(8): 1463 – 1471.
[6] Leisawitz D T, Danchi W C, DiPirro M J. Scientific motivation and technology requirements for the SPIRIT and SPECS far-infrared/submillimeter space interferometers[J]. 2000, **4013**: 36 – 46.
[7] de Bernardis P null, Ade P A, Bock J J. A flat Universe from high-resolution maps of the cosmic microwave background radiation [J]. *Nature*, 2000, **404**(6781): 955 – 959.
[8] Sean McHugh, Benjamin A. Mazin, Bruno Serfass, et al；A readout for large arrays of microwave kinetic inductance detectors. Rev. Sci. Instrum. 1 April 2012; 83 (4): 044702.
[9] Probst S, Song F B, Bushev P A. Efficient and robust analysis of complex scattering data under noise in microwave resonators[J]. *Review of Scientific Instruments*, 2015, **86**(2): 024706.
[10] Yates S J C, Baryshev A M, Baselmans J J A. Fast Fourier transform spectrometer readout for large arrays of microwave kinetic inductance detectors[J]. *Applied Physics Letters*, American Institute of Physics, 2009, **95**(4): 042504.
[11] Fruitwala N, Strader P, Cancelo G. Second generation readout for large format photon counting microwave kinetic inductance detectors [J]. *Review of Scientific Instruments*, American Institute of Physics, 2020, **91**(12): 124705.
[12] Nicholas Zobrist, Byeong Ho Eom, Peter Day, et al. Wide-band parametric amplifier readout and resolution of optical microwave kinetic inductance detectors. Appl. Phys. Lett.2019; 115 (4): 042601